Article

Not peer-reviewed version

Non-Intrusive Electrical Monitoring for Real-Time Estimation of the Production Parameters in a Sheet Metal Stamping Line

Camilo Carrillo González * , Eloy Díaz Dorado , Adrián Juan Pérez Peña , José Cidrás Pidre , Cristina Isabel Martínez Castañeda , José Florencio Sánchez Rúa

Posted Date: 13 March 2026

doi: 10.20944/preprints202603.1084.v1

Keywords: industrial electrical monitoring; energy patterns; nonintrusive load monitoring; machine learning; part classification

Article

Non-Intrusive Electrical Monitoring for Real-Time Estimation of the Production Parameters in a Sheet Metal Stamping Line

Camilo Carrillo González [1,*], Eloy Díaz Dorado [1], Adrián Juan Pérez Peña [1], José Cidrás Pidre [1], Cristina Isabel Martínez Castañeda [2] and José Florencio Sánchez Rúa [2]

[1] Research Group on Efficient and Digital Engineering, University of Vigo (Spain)
[2] Stellantis Group, 36210 Vigo, Spain
* Correspondence: Camilo Carrillo, carrillo@uvigo.es, University of Vigo, Vigo, Pontevedra 36310, Spain

Featured Application

This paper presents a non-intrusive, real-time method for identifying the part being produced in a metal stamping line and for estimating both cycle time and per-cycle energy consumption. The approach integrates machine-learning techniques, specifically Support Vector Machine (SVM) classification supported by features extracted from time-domain descriptors and Continuous Wavelet Transform (CWT) analysis.

Abstract

Metal forming processes play a key role in modern manufacturing, but they are characterized by high energy consumption and low overall efficiency. In this context, precise methods for monitoring the operational state and cycle-dependent metrics of manufactured parts are essential to implement energy optimization strategies. This article presents a data-driven and non-intrusive methodology to identify, in real time, the part under production and to estimate both cycle time and energy consumption per part. The method relies exclusively on electrical measurements taken at the main switchboard and at the first process-stage switchboard. These signals are used to calculate electrical quantities such as root mean square (RMS) current and active power, and a machine-learning (ML) approach is proposed to automatically identify the part in production. To this end, time-domain features are extracted directly from the signals, while time-frequency features are extracted using Continuous Wavelet Transform (CWT). These features are employed to train Support Vector Machine (SVM) classifiers optimized via grid search. Experimental results show that the model achieves a test accuracy of 99.9%. Once the production state is identified, the system estimates cycle time and energy per cycle in real time. Approximately 58,000 production cycles, corresponding to several part types were characterized.

Keywords: industrial electrical monitoring; energy patterns; nonintrusive load monitoring; machine learning; part classification

1. Introduction

Metal forming is a fundamental process in manufacturing, particularly in sectors such as vehicle production and aviation [1]. Such operations are characterized by high energy consumption due to the low efficiency of the metal forming presses [2]. In this context, monitoring consumption is essential in order to optimize efficiency, especially if, as this article proposes, the part in production is detected along with its cycle time and the energy per cycle.

Previous works of the research group, see [3,4], have shown that detailed analysis of metal forming presses from electrical measurements and the use of machine learning (ML) techniques have enabled identification of both the operating state of the presses and a breakdown of the energy

 doi:10.20944/preprints202603.1084.v1

consumed per cycle to give a precise characterization of the machine's dynamic behavior. This approach falls within a broader trend to use ML to monitor manufacturing processes. In [5] convolutional neural networks (CNNs) use electrical signals to identify the operational state of the painting sector in a vehicle factory and so more easily recognize specific events of interest. In [6] CNNs are also used to classify processes from acoustic signals in turning operations. The accumulated evidence indicates that these methodologies contribute significantly to the detailed analysis and energy improvement of manufacturing processes. However, joint application of high-speed electrical data acquisition and ML for energy estimation per cycle in sheet metal stamping presses remains an under-explored field.

Power quality analyzers commonly comply with the IEC 61000-4-30 standard [7] which establishes minimum intervals of ten cycles (for a 50 Hz power system) when calculating magnitudes such as root mean square (RMS) current or RMS voltage. Although this requirement is adequate for electrical supply supervision, it does not record in sufficient detail the rapid current variations that occur throughout the different phases of the metal forming cycle. These short-lived phenomena, associated with abrupt load changes (such as the mechanical impact during part forming) contain relevant information not only on the machine's operational state but also on its instantaneous energy behavior. Therefore, limited acquisition at ten-cycle intervals can lead to an underestimation of the effective energy consumed, and a loss of useful information for accurately identifying working regimes.

With the aim of addressing the limitations of conventional measurement systems and advance in the energy characterization of metal forming presses, this study presents the development of a high-speed electrical parameter measurement system capable of real-time processing, designed specifically to acquire voltage and current signals in sheet metal stamping lines. The system enables automatic classification of the production state using ML techniques and provides real-time estimates of both the cycle time and the associated energy consumption.

The article is organized as follows: Section 2 describes the electrical parameters measurement system developed; Section 3 details the preparation of the datasets and the classification procedure; Section 4 presents the estimation methods for the cycle time and its associated energy; Section 5 shows the results obtained; and, finally, Section 6 contains the conclusions.

2. Electrical Parameter Measurement System

The sheet metal stamping line analyzed in this article is fed from a main switchboard which has four dependent electrical panels that supply various subprocesses or stamping stages. To obtain the line's total consumption, current probes (Rogowski type) and a voltage probe were installed in the main switchboard (see Figure 1). Furthermore, to facilitate detection of the part in production, a current probe was installed in the switchboard of the first process stage. The voltage and current signals were sent to a data-acquisition system (DAQ) and a processing unit (CPU) which was responsible for real-time energy calculations, cycle-time estimation and part detection. The measurement system also had a display interface that allowed the results to be monitored. The main features of the equipment developed are shown in Table 1, which highlights the high speed of the power and RMS value calculations as well as its capacity to implement algorithms for detecting parts in production, with their corresponding cycle time and energy.

This equipment enabled the development of non-intrusive detection systems for the production characteristics of a specific process, such as the stamping line addressed in this article, which allowed implementation even without halting the installation from operating.

Preprints.org (www.preprints.org) | NOT PEER-REVIEWED | Posted: 13 March 2026 doi:10.20944/preprints202603.1084.v1

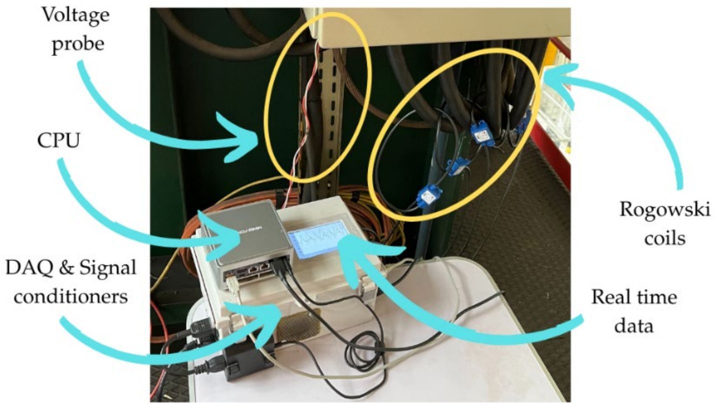

Figure 1. Measurement system for electrical parameters installed together with the stamping line main switchboard.

Table 1. Main characteristics of the measurement system.

Nº of channels	5
Current probes	4
Voltage probes	1
Sampling Rate	20 kHz
RMS and Power Rate	20 ms
CPU	Intel Core i9-12900H
RAM	32 GB
Storage	1 TB

3. Dataset Preparation and Classification

3.1. Characterization and Time Segmentation

Initial analysis of the current signals acquired showed a behavior that, although cyclical in both cases, was markedly non-stationary on the main switchboard (attributable to the aggregate nature of the consumption by multiple pieces of equipment) and more stable on the first process-stage switchboard. Figure 2 shows an example of the current signals acquired simultaneously on both switchboards during several production cycles while forming a part.

In order to structure the signals for processing compatible with real-time implementation, they were segmented into 20-second windows. This duration was chosen after verifying that the typical production cycle time ranged between five and seven seconds per part, which ensured that each window contained at least two complete cycles.

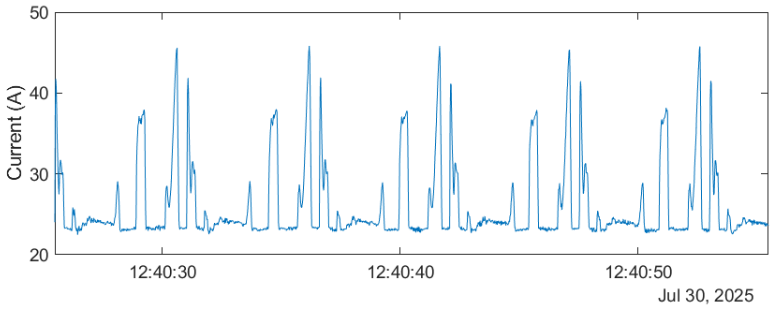

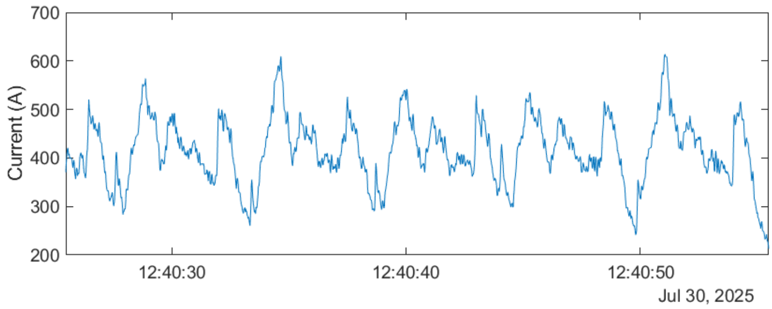

Figure 2. Time variation of the RMS current measured simultaneously on the main switchboard (bottom) and the first process-stage switchboard (top).

3.2. Dataset Labelling and Construction

To permit dataset construction, the company provided the part reference being produced at each time instant, which made it possible to associate a label to each 20-second window corresponding to the manufactured part. Although nine distinct parts or references were analyzed (P1 to P9), a total of ten classes were used: the nine identified parts and an additional class called “idle” (IDLE), which was assigned to those windows in which no part was being processed. The inclusion of this class prevented the classifier from unduly assigning unproductive periods to a specific part and enabled detection of inactive states, a necessary requirement for the subsequent calculation of cycle-dependent metrics, such as the cycle time.

Despite data being compiled for model construction over three months, actual production was not evenly distributed to reflect the different classes and so some parts appear more often than others. To avoid bias while training the classifiers, the dataset was balanced by randomly downsampling the majority classes until an equal number of samples per class was reached.

A total of seven thousand 20-second windows were used for feature extraction, with 700 representations of each class, using information from both the main switchboard and the first process-stage switchboard.

3.3. Feature Extraction in the Time and Time-Frequency Domains

To address the variability of the current signals within each window, classic spectral analysis methods such as the Fourier Transform are insufficient as they assume stationarity and do not adequately capture time-varying frequency components [8].

A common alternative for analyzing non-stationary signals is the Short-Time Fourier Transform, based on the application of a sliding window on the signal. Although this technique provides information in both the time and the frequency domains, it has a fundamental limitation: the window size is fixed, which imposes a constant time or frequency resolution throughout the signal. This approach is not suitable for highly dynamic processes, where the aim is to capture with precision both time information in high-frequency transients and more persistent patterns in low-frequency bands [9].

To overcome this trade-off between time and frequency resolution, the Continuous Wavelet Transform (CWT) was employed, as it has been shown to outperform other techniques in the analysis of non-stationary signals [6,10]. The CWT calculates the similarity between the signal and a base function (mother wavelet) shifted and scaled in time (wavelet), which enables adaptive decomposition: the small scales correspond to high-frequency components, while the large scales represent low frequency variations [11]. These scales are logarithmically distributed, and the choice of their density introduces a trade-off between frequential resolution and computational cost.

In this study, the Morlet wavelet was chosen as the mother wavelet as it represents the best balance between time and frequency resolution [12]. Analysis was performed using the MATLAB Wavelet Toolbox [13], setting a value of four voices per octave to control the scale density. With this information and the ratio to obtain the RMS values (50 Hz), the software automatically determined

Preprints.org (www.preprints.org) | NOT PEER-REVIEWED | Posted: 13 March 2026 doi:10.20944/preprints202603.1084.v1

the range of frequencies considered, which in this case spanned from approximately 0.14 to 18.41 Hz, leading to a total of 29 scales (seven octaves in addition to the minimum scale). Statistical features were extracted from the coefficients obtained in each scale: mean, skewness, kurtosis, RMS and variance. Previous studies [14,15] have demonstrated the effectiveness of such statistical features derived from wavelet coefficients when representing non-stationary dynamics.

Furthermore, to enhance signal representation, some of the most commonly used descriptors from the time domain were included in the classification: mean, range, RMS, variance, skewness and kurtosis.

3.4. Normalization and Partitioning

After feature extraction, each dataset was divided into two subsets: 85% of the samples were used for training and validation, while the remaining 15% were reserved for final testing.

Since the extracted features exhibited heterogeneous numerical ranges, Z-score normalization was applied [16]. The normalization parameters (mean and standard deviation) were computed using only the training data and subsequently applied to the test set, ensuring that no information leakage occurred.

Figures 3 and 4 show the scatter plots of the training samples for both datasets, indicating the part in production (P1 to P9) and the idle state (IDLE). The figures show better separation in the classes corresponding to the current probe installed at the first process-stage switchboard compared to those obtained from the current probe installed at the main switchboard.

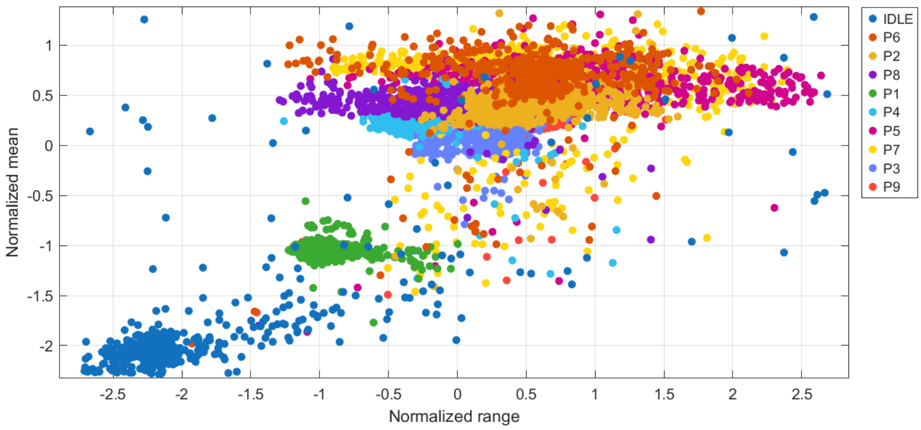

Figure 3. Scatter plot of two normalized time-domain features from the main switchboard training dataset: mean and range.

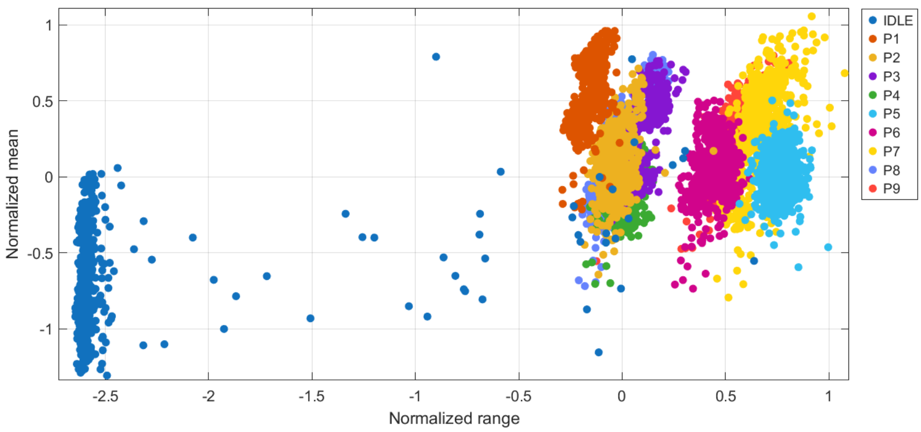

Figure 4. Scatter plot of two normalized time-domain features from the first process-stage training dataset: mean and range.

 doi:10.20944/preprints202603.1084.v1

3.5. Classification using SVM

Support Vector Machines (SVM) are supervised learning models that have demonstrated strong performance in both regression and classification problems [17]. This model is based on the creation of a hyperplane that maximizes the margin between classes [18].

To fit the model to both datasets, the hyperparameters were tuned, since they control the model's learning process and cannot be learnt from the data [19]. To this end, a grid search was used in combination with cross validation [20,21]. Grid search is an exhaustive search technique that evaluates different combinations of hyperparameters within a predefined space [22,23]. In this study, the error in classification was calculated for each hyperparameter combination by means of five-fold cross validation, finally selecting the set that minimized this error.

The search space included the kernel function (linear, polynomial and radial basis function (RBF)); the cost parameter (C), explored on a logarithmic scale from 0.001 to 1000, and the gamma parameter (γ) which was explored over the same range (only considered in the case in which the kernel function was RBF).

All the models were trained using features previously normalized by means of Z-score, following the procedure described in Section 3.4. The multiclass classification was implemented using the one-vs-one decomposition, a strategy recommended because of its good performance in multiclass problems [24].

The structure and specifications of both models are summarized in Table 2.

Table 2. Summary of the configuration used to train both SVM models, including the hyperparameter search space evaluated using grid search.

Parameter	Configuration
Kernel function	Linear, Polynomial (degree 2,3), RBF (optimized via grid search)
Cost (C)	0.001–1000 (log-spaced, optimized via grid search)
Gamma (γ, only for RBF)	0.001–1000 (log-spaced, optimized via grid search)
Normalization	Z-score
Multiclass strategy	One-vs-One
Train–Test split	85–15

4. Cycle Time and Energy Estimation Per Part

4.1. Cycle Time Estimation

Once the model predicted that a part was being stamped, the RMS current measured at the first process-stage switchboard was used to estimate the cycle time, as this presented a more stable and repetitive structure than the aggregated measurements from the main switchboard. This facilitated the identification of the stamping cycles.

A peak-detection algorithm was applied to this signal, using minimum peak height and minimum peak distance criteria to identify the most representative event of each cycle. In this way, the cycle time is the time lapse between two consecutive events. Figure 5 shows an example of the procedure applied.

doi:10.20944/preprints202603.1084.v1

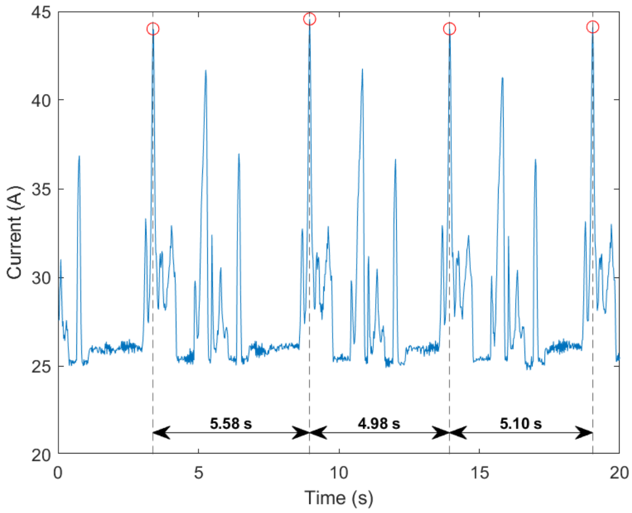

Figure 5. Example of peak detection applied to the current signal measured at the first process-stage switchboard for cycle time estimation.

4.2. Energy Estimation Per Produced Part

To estimate the energy associated with each cycle, the timestamps of the detected peaks were synchronized with the aggregated active power measured on one phase of the main switchboard, as both signals were acquired simultaneously and shared the same timestamp.

Additional measurements from a power quality analyzer were used to verify that consumption in the three phases was balanced and that the power factor was close to unity. Therefore, the total energy absorbed in each cycle was calculated from the active power measured between two consecutive peaks, the result of which was subsequently multiplied by the number of phases. An example of this synchronization between both signals can be seen in Figure 6.

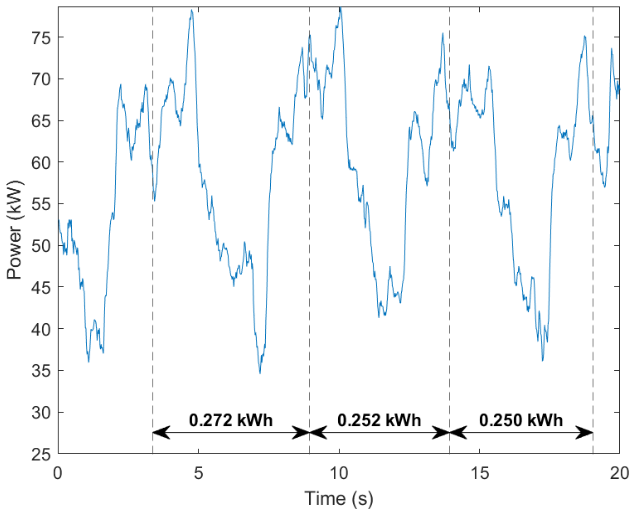

Figure 6. Example of the energy estimation in each production cycle obtained through synchronization between cycle events and active power measurements.

5. Results

5.1. Estimation of the Line State

Hyperparameter optimization by grid search produced, for both datasets, SVM models with linear kernels. The final values selected for each model are given in Table 3.

 doi:10.20944/preprints202603.1084.v1

Table 3. Hyperparameters selected for the SVM models by grid search.

	Main switchboard	First process-stage switchboard
Kernel function	Linear	Linear
Cost (C)	0.2512	0.0158

Model performance was evaluated on the reserved test set. The classifier trained on aggregated measurements from the main switchboard achieved a test accuracy of 96%. Its confusion matrix (Figure 7) shows limited separability among certain classes, particularly parts P5, P6, and P7. In contrast, the model trained on disaggregated measurements from the first process-stage switchboard reached a test accuracy of 99.9%, with only a single misclassified sample. Its confusion matrix is shown in Figure 8.

Altogether, the results confirm that disaggregated electrical measurements, based on adding a current sensor at the first process-stage switchboard, offer greater discriminative capability for line-state classification. Therefore, this signal was selected for subsequent real-time part identification and cycle-level analysis.

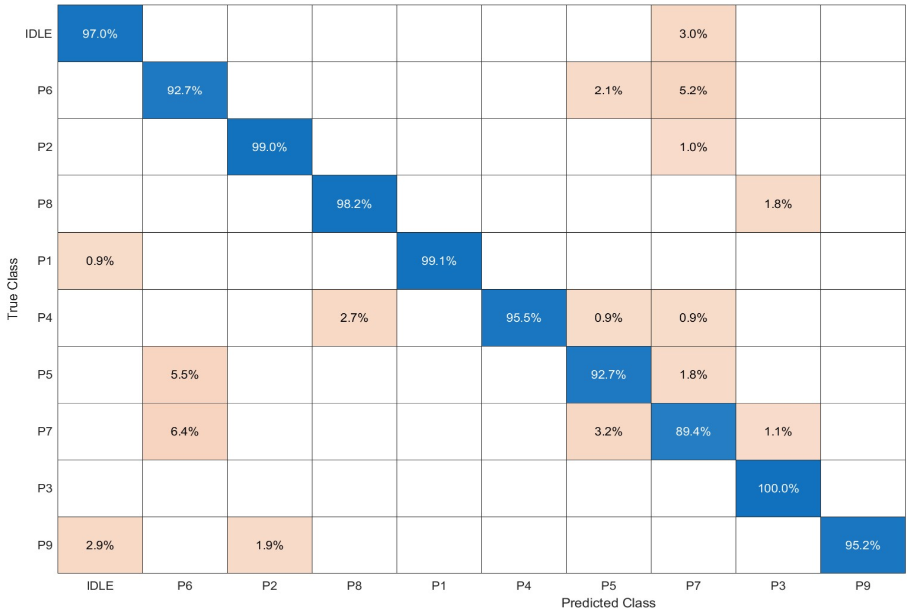

Figure 7. Confusion matrix of the SVM model for the test set corresponding to the main switchboard.

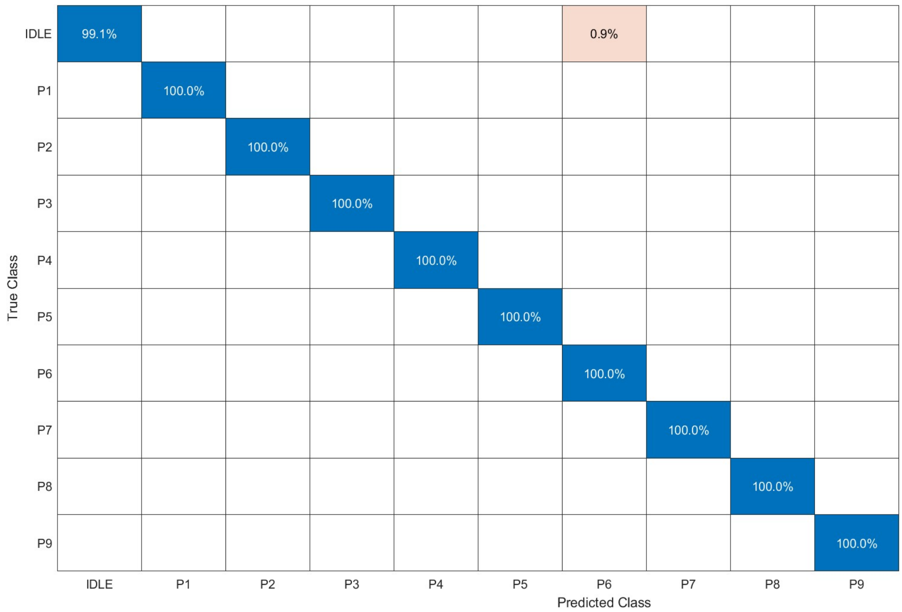

Figure 8. Confusion matrix of the SVM model for the test set corresponding to the first process-stage switchboard.

5.2. Estimation of Cycle Time and Energy Per Cycle

From the classification undertaken on the data acquired over 18 days of operation, approximately 58,000 production cycles were identified. Both the cycle time and the demanded energy were estimated for each cycle, following the procedure described in Sections 4.1 and 4.2.

Figure 9 gives the cycle-time boxplots by part type, revealing differences in both the median cycle time and its dispersion.

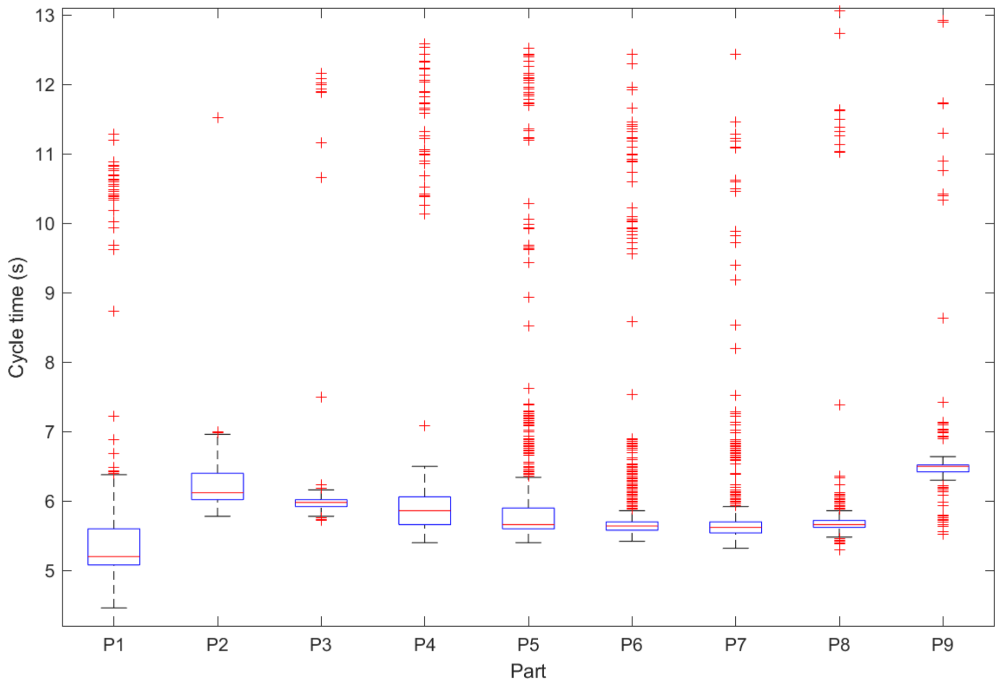

Figure 9. Boxplots of cycle time by part type. Each box represents the interquartile range (IQR) and the median; whiskers extend to 1.5·IQR and the outer points correspond to outliers.

To complement the graphic analysis, Table 4 summarizes the main descriptive statistics for the cycle time by part type, while Table 5contains the values corresponding to the electrical energy consumed per cycle. In both cases, the mean is shown along with the 5th and 95th percentiles, which makes it possible to characterize the behavior and variability of each part.

Figure 10 shows the energy consumed against cycle time, where a growing relationship between both magnitudes can be seen. This relationship can be adequately approximated by a linear model. To quantify this behavior, the coefficient of determination R^2 was evaluated for each part type, obtaining values that ranged between 0.79 and 0.96, which confirms a marked linear dependency between both variables.

Figure 11 and Figure 12 depict two representative examples corresponding to the cases with the smallest and largest value of R^2, respectively.

Table 4. Descriptive statistics (mean and percentiles 5% and 95%) of the cycle time by part type.

Part	Mean (s)	P05 (s)	P95 (s)
P1	5.36	4.96	5.70
P2	6.28	5.94	6.80

P3	6.01	5.84	6.08
P4	5.90	5.56	6.16
P5	5.82	5.52	6.30
P6	5.72	5.46	6.04
P7	5.81	5.46	6.70
P8	5.70	5.54	5.86
P9	6.53	6.40	6.60

Table 5. Descriptive statistics (mean and percentiles 5% and 95%) of the electrical energy consumed per cycle and part type.

Part	Mean (kWh)	P05 (kWh)	P95 (kWh)
P1	0.269	0.252	0.285
P2	0.453	0.430	0.478
P3	0.402	0.382	0.415
P4	0.412	0.383	0.442
P5	0.438	0.415	0.465
P6	0.436	0.412	0.467
P7	0.450	0.392	0.520
P8	0.413	0.397	0.431
P9	0.461	0.442	0.487

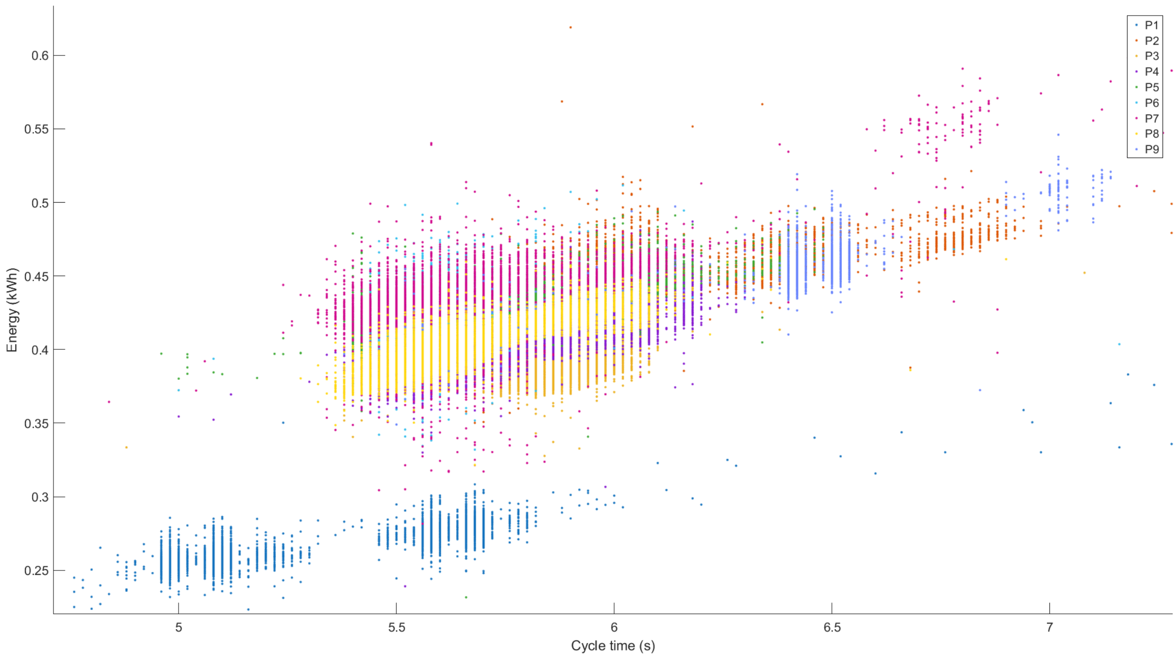

Figure 10. Scatter plot for the energy consumed against cycle time.

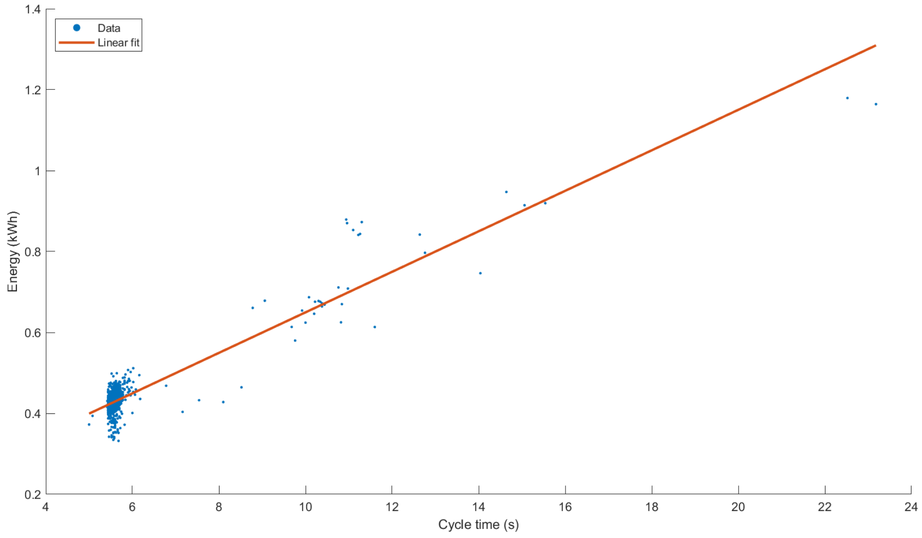

Figure 11. Relationship between energy consumed and cycle time for the part with smallest determination coefficient: P6 ($R^2 = 0.79$).

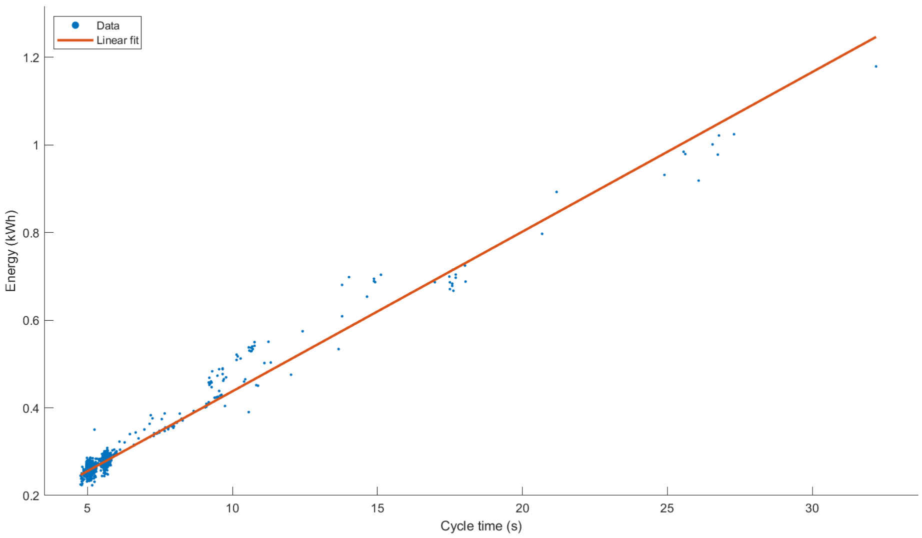

Figure 12. Relationship between energy consumed and cycle time for the part with largest determination coefficient: P1 ($R^2 = 0.96$).

5.3. Real-Time Operation

The Figure 13 shows screenshots extracted from [25] corresponding to the electrical parameter measurement system display interface during real-time operation. The interface provides an integrated real-time visualization of electrical signals acquired from both switchboards, the classification result (the part in production), the detected production cycles, and their duration (cycle time) and associated energy.

Preprints.org (www.preprints.org) | NOT PEER-REVIEWED | Posted: 13 March 2026 doi:10.20944/preprints202603.1084.v1

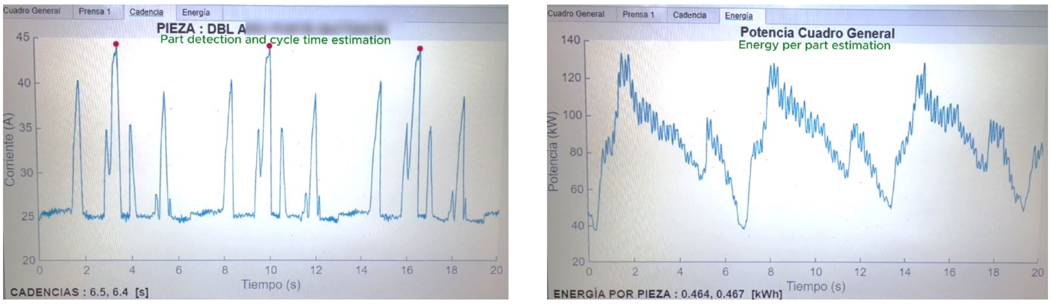

Figure 13. Real-time screen capture of the developed system in operation within the plant.

6. Conclusions

This study develops and implements a high-speed measurement system for electrical parameters capable of obtaining values for power and RMS every 20 ms in addition to allowing the implementation of algorithms to characterize parts in production in real time.

The detection algorithm for parts in production only uses the current signals acquired by the monitoring system. Features from the time-frequency domain are extracted from those signals (via CWT) as are those from the time domain to train SVM classifiers, whose hyperparameters were selected by grid search to identify the state of the line. The resulting models show notable performance, particularly in the disaggregated dataset (corresponding to the first process stage), where a test accuracy of 99.9% was reached.

Once the state of the line was identified, a peak-detection algorithm was applied to estimate the cycle time. As the electrical measurements from both switchboards were synchronized, it was possible to associate each cycle with its individual energy consumption.

This procedure allowed disaggregation in real time to be acquired for the part in production, obtaining both its cycle time and the energy consumed. In this way, through non-intrusive techniques and the use of ML algorithms (SVM with Linear Kernel), a quantitative basis was provided that enabled verification of the production line's operation and optimization of the energy demand.

Author Contributions: Conceptualization, C.C.G. and E.D.D.; Methodology, C.C.G., E.D.D., A.J.P.P. and J.C.P.; Software, A.J.P.P.; Validation, C.C.G., E.D.D. and A.J.P.P.; Formal analysis, C.C.G., E.D.D. and A.J.P.P.; Investigation, C.C.G., E.D.D. and A.J.P.P.; Data curation, A.J.P.P.; Resources, C.I.M.C. and J.F.S.R.; Visualization, A.J.P.P.; Writing—original draft preparation, A.J.P.P.; Writing—review and editing, C.C.G., E.D.D., J.C.P., C.I.M.C. and J.F.S.R.; Supervision, C.C.G. and E.D.D.; Project administration, C.C.G.; Funding acquisition, C.C.G. All authors have read and agreed to the published version of the manuscript.

Funding: The activities described in this article were carried out within the framework of the project "Facendo Plus (Factory Competitiveness and Electromobility Through Innovation and Digital Transformation Plus)" (IN854A 2023/01), funded by the European Regional Development Fund under the Feder Galicia 2021–2027 programme.

Institutional Review Board Statement: Not applicable.

Informed Consent Statement: Not applicable.

Data Availability Statement: The data presented in this study are not publicly available due to confidentiality agreements with the industrial partner where the measurements were conducted.

Conflicts of Interest: The authors declare no conflict of interest.

References

1. J. Zhong, K. Zhao, Z. Liu, and X. Li, "Review of the research on low carbon manufacture of metal-forming equipment and future development," *J. Hefei Univ. Technol.(Nat. Sci.)*, vol. 35, no. 12, pp. 1594–1600, 2012.

2. M. Gao, K. He, L. Li, Q. Wang, and C. Liu, "A review on energy consumption, energy efficiency and energy saving of metal forming processes from different hierarchies," Jun. 01, 2019, *MDPI AG*. https://doi.org/10.3390/pr7060357.
3. C. Carrillo *et al.*, "Detailed Energy Analysis of a Sheet-Metal-Forming Press from Electrical Measurements," *Energies (Basel).*, vol. 16, no. 19, Oct. 2023. https://doi.org/10.3390/en16196972.
4. C. Carrillo-González *et al.*, "Análisis mediante redes neuronales del perfil energético de una prensa de conformado de chapa en el sector de la automoción," *Revista Iberoamericana de Ingeniería Mecánica*, vol. 27, no. 2, pp. 17–33, Sep. 2023. https://doi.org/10.5944/ribim.27.2.42141.
5. A. Verma, S.-C. Oh, J. Arinez, and S. Kumara, "Hierarchical energy signatures using machine learning for operational visibility and diagnostics in automotive manufacturing," 2024. https://doi.org/10.48550/arXiv.2402.15962.
6. Y. Liao, I. Ragai, Z. Huang, and S. Kerner, "Manufacturing process monitoring using time-frequency representation and transfer learning of deep neural networks," *J. Manuf. Process.*, vol. 68, pp. 231–248, Aug. 2021. https://doi.org/10.1016/j.jmapro.2021.05.046.
7. International Electrotechnical Commission, "Electromagnetic compatibility (EMC) - Part 4-30: Testing and measurement techniques - Power quality measurement methods," 2015.
8. C. J. Carrillo González, "Fundamentos del Análisis de Fourier," 2003.
9. M. Ge, G. C. Zhang, R. Du, and Y. Xu, "Feature extraction from energy distribution of stamping processes using wavelet transform," *JVC/Journal of Vibration and Control*, vol. 8, no. 7, pp. 1023–1032, 2002. https://doi.org/10.1177/107754602029577.
10. D. Łuczak, "Mechanical Vibrations Analysis in Direct Drive Using CWT with Complex Morlet Wavelet," *Power Electronics and Drives*, vol. 8, no. 1, pp. 65–73, Jan. 2023. https://doi.org/10.2478/pead-2023-0005.
11. R. X. Gao and R. Yan, *Wavelets: Theory and Applications for Manufacturing*. Springer Science & Business Media, 2010.
12. L. A. Conraria and M. J. Soares, "The continuous wavelet transform: A primer," 2011.
13. T. M. Inc., "Wavelet Toolbox version: 25.1 (R2025a)," 2025, *The MathWorks Inc., Natick, Massachusetts, United States*. [Online]. Available: https://www.mathworks.com/products/wavelet.html
14. P. Konar, M. Saha, J. Sil, and P. Chattopadhyay, "Fault diagnosis of induction motor using CWT and rough-set theory," in *2013 IEEE Symposium on Computational Intelligence in Control and Automation (CICA)*, 2013, pp. 17–23. https://doi.org/10.1109/CICA.2013.6611658.
15. M. Chandani, "Statistical Wavelet Features, PCA, MLPNN, SVM and K-NN Based Approach for the Classification of EEG Physiological Signal," *International Journal of Industrial and Manufacturing Systems Engineering*, vol. 2, no. 5, p. 57, 2017. https://doi.org/10.11648/j.ijimse.20170205.12.
16. M. Sholeh and E. K. Nurnawati, "Comparison of Z-score, min-max, and no normalization methods using support vector machine algorithm to predict student's timely graduation," *AIP Conf. Proc.*, vol. 3077, no. 1, p. 40003, Feb. 2024. https://doi.org/10.1063/5.0202505.
17. D. Mustafa Abdullah and A. Mohsin Abdulazeez, "Machine Learning Applications based on SVM Classification A Review," *Qubahan Academic Journal*, vol. 1, no. 2, pp. 81–90, Apr. 2021. https://doi.org/10.48161/qaj.v1n2a50.
18. S. B. Kotsiantis, "Supervised Machine Learning: A Review of Classification Techniques," 2007.
19. M. Y. Shams, A. M. Elshewey, E. S. M. El-kenawy, A. Ibrahim, F. M. Talaat, and Z. Tarek, "Water quality prediction using machine learning models based on grid search method," *Multimed. Tools Appl.*, vol. 83, no. 12, pp. 35307–35334, Apr. 2024. https://doi.org/10.1007/s11042-023-16737-4.
20. M. Adnan, A. A. S. Alarood, M. I. Uddin, and I. ur Rehman, "Utilizing grid search cross-validation with adaptive boosting for augmenting performance of machine learning models," *PeerJ Comput. Sci.*, vol. 8, 2022. https://doi.org/10.7717/PEERJ-CS.803.
21. F. Budiman, "SVM-RBF parameters testing optimization using cross validation and grid search to improve multiclass classification," *Scientific Visualization*, vol. 11, no. 1, pp. 80–90, 2019. https://doi.org/10.26583/sv.11.1.07.

 doi:10.20944/preprints202603.1084.v1

22. M. A. Nanda, K. B. Seminar, D. Nandika, and A. Maddu, "A comparison study of kernel functions in the support vector machine and its application for termite detection," *Information (Switzerland)*, vol. 9, no. 1, Jan. 2018. https://doi.org/10.3390/info9010005.
23. M. A. Haqmi Abas, "Agarwood Oil Quality Classification using Support Vector Classifier and Grid Search Cross Validation Hyperparameter Tuning," *International Journal of Emerging Trends in Engineering Research*, vol. 8, no. 6, pp. 2551–2556, Jun. 2020. https://doi.org/10.30534/ijeter/2020/55862020.
24. C.-W. Hsu and C.-J. Lin, "A comparison of methods for multiclass support vector machines," *IEEE Trans. Neural Netw.*, vol. 13, no. 2, pp. 415–425, 2002. https://doi.org/10.1109/72.991427.
25. A. J. Pérez Peña, C. Carrillo Gonzalez, and E. Díaz-Dorado, "Real-Time Detection of Parts, Cadence, and Energy per Part ," Dec. 2025, *Zenodo*. https://doi.org/10.5281/zenodo.17951482.